### Title

Three-Dimensional Reconstruction of Skeletal Muscle Extracellular Matrix Ultrastructure




### Journal

Microscopy and Microanalysis, 20(6)

### ISSN

1431-9276



### Authors

Gillies, Allison R
Bushong, Eric A
Deerinck, Thomas J
et al.



### Publication Date

2014-12-01

### DOI

10.1017/s1431927614013300

Peer reviewed

Published in final edited form as:
*Microsc Microanal*. 2014 December ; 20(6): 1835–1840. doi:10.1017/S1431927614013300.

# Three-dimensional reconstruction of skeletal muscle extracellular matrix ultrastructure

**Allison R. Gillies**[1], **Eric A. Bushong**[2], **Thomas J. Deerinck**[2], **Mark H. Ellisman**[2,3], and **Richard L. Lieber**[1,4]

[1]Department of Bioengineering, University of California San Diego, La Jolla, CA

[2]National Center for Microscopy and Imaging Research, University of California San Diego, La Jolla, CA

[3]Department of Neurosciences, University of California San Diego, La Jolla, CA

[4]Department of Orthopaedic Surgery, University of California San Diego, Jolla, CA

## Abstract

The skeletal muscle extracellular matrix (ECM) supports muscle's passive mechanical function and provides a unique environment for extracellular tissues such as nerves, blood vessels and a cadre of mononuclear cells. Within muscle ECM, collagen is thought to be the primary load bearing protein, yet its structure and organization with respect to muscle fibers, tendon, and mononuclear cells is unknown. Detailed examination of extracellular collagen morphology requires high-resolution electron microscopy performed over relatively long distances because multinucleated muscle cells are very long and extend from several millimeters to several centimeters. Unfortunately, there is no tool currently available for high resolution ECM analysis that extends over such distances relevant to muscle fibers. Serial block face scanning electron microscopy (SBEM) is reported here for the first time to examine skeletal muscle ECM ultrastructure over hundreds of microns. Ruthenium red staining was implemented to enhance contrast and utilization of variable pressure imaging reduced electron charging artifacts, allowing continuous imaging over a large ECM volume. This approach has revealed previously unappreciated perimysial collagen structures that were reconstructed via both manual and semi-automated segmentation methods. Perimysial collagen structures in the ECM may provide a target for clinical therapies aimed at reducing skeletal muscle fibrosis and stiffness.

Correspondence to: Richard L. Lieber.

Allison R. Gillies, PhD, 9500 Gilman Drive, La Jolla, CA 92093-0863, Phone: 858-822-8502, Fax: 858-822-3807, agillies@ucsd.edu
Eric A. Bushong, PhD, 9500 Gilman Drive, La Jolla, CA 92093-0608, Phone: 858-534-0276, Fax: 858-534-7497, eric@ncmir.ucsd.edu
Thomas J. Deerinck, 9500 Gilman Drive, La Jolla, CA 92093-0608, Phone: 858-534-0276, Fax: 858-534-7497, deerinck@ncmir.ucsd.edu
Mark H. Ellisman, PhD, 9500 Gilman Drive, La Jolla, CA 92093-0608, Phone: 858-534-0276, Fax: 858-534-7497, mark@ncmir.ucsd.edu
Richard L. Lieber, PhD, 9500 Gilman Drive, La Jolla, CA 92093-0863, Phone: 858-822-1344, Fax: 858-822-3807, rlieber@ucsd.edu

**Keywords**

Skeletal muscle; extracellular matrix; collagen; serial block face scanning electron microscopy; perimysium

## Introduction

Electron microscopic methods for examining biological tissues were developed, in large part, for studies of skeletal muscle (Richards et al., 1942; Sjöstrand, 1943). Such reports date back to the 1940s with the first structural investigation of myofibrils (Hall et al., 1946). Historically, skeletal muscle ultrastructural studies that focused on muscle fibers (Hall, et al., 1946; Huxley & Hanson, 1954), sarcoplasmic reticulum and T-system (Eisenberg et al., 1974), and the neuromuscular junction (Rash & Ellisman, 1974) were limited to a few thin sections along the fiber length. In contrast to the contractile and regulatory machinery of muscle fibers, the structure of the skeletal muscle extracellular matrix (ECM) has received far less attention. Skeletal muscle ECM is traditionally subdivided into endomysium, perimysium, and epimysium based upon cross-sectional morphology, but these subdivisions are relatively arbitrary and, in very few cases, are any structural or biochemical differences among regions actually specified. There are, however, notable exceptions to this oversight. In the early 1980s, the endomysial collagen network and large collagen bundles in the perimysium of several muscles were described (Borg & Caulfield, 1980; Rowe, 1981). The arrangement and orientation of endomysial collagen fibrils were quantified as a function of sarcomere length to yield a model of load bearing during passive muscle stretch (Purslow & Trotter, 1994; Trotter & Purslow, 1992). More recently, perimysial junctional plates were described in which very large collagen bundles appear to traverse great distances and “insert” onto muscle cells at discrete locations along the fiber (Passerieux et al., 2006).

The primary reason that skeletal muscle ECM has not been thoroughly studied is that it has been viewed as largely inert, providing only a supporting role to the more significant contractile muscle fibers. However, recent reports have highlighted that, in response to perturbation, it is actually the ECM that shows a greater degree of adaptation compared to muscle fibers. For example, in response to intracellular deletion of the intermediate filament desmin, it is actually the extracellular connective tissue matrix that shows the greatest degree of adaptation (Meyer & Lieber, 2012). Further, in children with cerebral palsy, while muscle fiber size decreases slightly, the ECM proliferates and becomes deranged, which appears to be responsible for much of the clinical manifestations of this musculoskeletal disorder (Smith et al., 2011). In these and similar cases, ECM structural changes that occur are not well understood and are typically simply described as a “thickening” or increase in area fraction of the endomysium and/or perimysium. These simplistic morphological measurements or measurements of total collagen content do not correlate well with tissue mechanical properties (Smith, et al., 2011).

Previous microscopy methods used to observe ECM are not sufficient to describe ECM ultrastructure because they lack resolution (immunohistochemistry, confocal microscopy), provide only a 2-dimensional view (transmission electron microscopy, TEM), do not

provide information over long distances, or preparation methods disrupt *in vivo* tissue organization (scanning electron microscopy, SEM). In this report, we show that, with the development of 3-dimensional imaging technology and improved staining techniques, it is now possible to detail skeletal muscle ECM ultrastructure over relatively large distances. Serial block face scanning electron microscopy (SBEM) combines the benefits of TEM-scale resolution and tissue structure preservation with the 3D visualization capability of SEM (Denk & Horstmann, 2004; Starborg et al., 2013). Imaging skeletal muscle ECM with SBEM presents specific challenges. Therefore the purpose of this study was to refine this method in order to enable studies of ECM architecture and plasticity. To our knowledge, this is the first application of SBEM to studies of skeletal muscle ECM structure.

## Materials and Methods

### Tissue Preparation and Staining

All work was approved by the UCSD IACUC prior to beginning. Fixation and embedding reagents were obtained from Electron Microscopy Sciences (Hartfield, PA). Wild type 129/SV mice (n=5) were anesthetized with intraperitoneal injection of either pentobarbital (100 mg/kg) or rodent cocktail (100 mg/kg ketamine, 10 mg/kg xylazine, 3 mg/kg acepromazine) and transcardially perfused with mammalian Ringers solution warmed to 35°C containing heparin (20 units/ml) and 0.2% dextrose for 2 minutes followed by 2% paraformaldehyde, 2.5%glutaraldehyde, 0.05% ruthenium red, and 0.2% tannic acid in 0.15M sodium cacodylate buffer containing 2mM calcium chloride at 35°C for 5 minutes. After complete fixation, extensor digitorum longus (EDL) muscles were dissected and incubated in the same fixative solution overnight at 4°C. Tissue was prepared using a modified version of the methods reported by West *et al.* (West et al., 2010). Briefly, tissues were washed with sodium cacodylate buffer followed by incubation in 2% osmium tetroxide containing 1.5% potassium ferrocyanide and 0.05% ruthenium red in 0.15M sodium cacodylate buffer for 30 minutes. Samples were washed in distilled water and incubated in 1% thiocarbohydrazide for 20 minutes. Tissues were then washed with distilled water, incubated in 2% osmium tetroxide for 30 minutes, washed with distilled water, and placed in 2% uranyl acetate overnight at 4°C. The following day, tissues were stained *en bloc* with Walton's lead aspartate for 15 minutes at 60°C followed by washing with distilled water and dehydration in graded ethanol. Finally tissues were embedded in Durcupan ACM resin (Sigma-Aldrich, St. Louis, MO), trimmed to $\sim 1 mm^3$ blocks and mounted onto aluminum pins.

### Serial Block Face Scanning Electron Microscopy

Specimens were placed into a Zeiss Sigma scanning electron microscope outfitted with a serial block face-imaging chamber (Gatan 3View, Pleasanton, CA). Digital Micrograph software (Gatan) was used to control knife and specimen movement within the chamber as well as to collect data. Images were obtained at 3kV accelerating voltage with a 60mm aperture under variable pressure (chamber pressure was varied from 28 to 35 Pa to offset specimen charging). Beam stigmation and aperture alignment were performed as necessary prior to data collection. Tissue blocks were sectioned at 70nm thickness. Images were recorded at 2,300× magnification and raster size 8,000 × 8,000 with 1μs dwell time,

resulting in a spatial resolution of 4.51 nm/pixel. Approximately 2,000 images were obtained during each session (extending a distance of ∼150μm), with focus and stigmation adjusted periodically during imaging. Cutting speed was set to 0.5mm/second with oscillation. Total sectioning time was ∼36 hours per tissue block.

### Image Processing

Images were converted to 8bit for analysis and binned by a factor of 6 prior to segmentation. Calculation of cross-correlation between adjacent images permitted alignment and stacking. Both manual and semi-automated segmentation methods were used to identify objects of interest including fibroblasts, capillaries, and grouped collagen fibrils (perimysial collagen cables). Initial attempts at segmentation were performed manually with IMOD software (Kremer et al., 1996). Manually drawn object contours were linearly interpolated over 10 images unless object branching or irregular changes in object shape and/or location necessitated drawing contours on each image. In a second approach, Analyze 11.0 software (Analyze Direct, Inc., Overland Park, KS) was also used to segment the same datasets. Objects were defined by thresholding a seed point close to the center of the object, and the seed point and threshold settings were propagated onto neighboring images to grow the object throughout the volume (Object Extractor tool). Voxel sizes depended upon imaging parameters. Manual corrections were performed in Analyze as necessary after object extraction completed.

## Results

A typical image of the extracellular space obtained from SBEM of EDL tissue is shown in Figure 1 (see Supplementary Movie 1 for serial images of the entire volume). Manual segmentation of all capillaries, fibroblasts, and perimysial collagen cables within the volume shown in Supplementary Movie 1, interpolating every ∼10 slices, required∼40 hours for an experienced user. Time required for semi-automated segmentation was highly variable, and depended on factors such as computer processor speed and available RAM, user expertise, and inherent properties of the volume (contrast between objects, object complexity, etc.). However, active user time totaled about 10 minutes per hour of semi-automated segmentation time. This is because user input was only required to set threshold parameters and select seed points; supervision was not required while the segmentation algorithm was running. Because segmentation of an object throughout the volume depended upon the thresholding parameters that were set independently for each seed point, multiple seed points were typically required to segment a single object. Approximately 20 hours of manual corrections were required after semi-automated segmentation was complete for a single sample. Thus, total user time for manual segmentation was ∼40 hours per volume, while with semi-automated segmentation, total user time was ∼33 hours per volume.

Direct comparison between manual and semi-automated segmentation results showed that Analyze was able to segment some collagen cables that could not be defined manually, but was unable to segment collagen cables that were in close proximity to objects with similar grayscale value (Fig. 2, arrows). While the same overall structures were identified between methods, three-dimensional reconstruction of manually and semi-automatically segmented

datasets differed in the appearance of their structure surfaces (Fig. 3). IMOD software applies a mesh over the manually defined contours giving the 3D reconstruction a smooth appearance, whereas individual voxels belonging to an object are highlighted in Analyze giving objects a more textured appearance (rotations of the IMOD and Analyze segmented 3D reconstructions are provided as Supplemental Movies 2 and 3, respectively).

Regarding ECM structure, final segmentation using either method yielded a surprisingly long network of collagen fibrils bundled together into “cables” that undulated along the tissue and, in some cases, split into multiple cables. Because the structure of these cables does not correspond to the traditional appearance of endomysium (Trotter & Purslow, 1992) as well as their location, we defined them to be perimysial collagen. Perimysial collagen cables appeared in close proximity to fibroblasts and were generally oriented along the muscle fiber axis. In addition to perimysial cables, fibroblasts were also segmented and their spatial proximity to perimysial cables was identified (Fig. 4). Long fibroblast processes were closely associated with perimysial cables across hundreds of microns of distance as well as the muscle fiber surface. Fibroblasts also formed long projections, but these projections did not appear to be the so-called fibripositors (Canty et al., 2004). Fibroblast projections were flat, wide and sheet-like or finger-like (Fig. 4). Their reconstruction reinforced the point that, to adequately appreciate fibroblast morphology, high-resolution reconstruction of extended distances is required.

## Discussion

Three-dimensional SBEM imaging of skeletal muscle has revealed high-resolution micro- and meso-scale structural information that was previously unappreciated. Because skeletal muscle ECM contains a large volume of non-electron dense space, it presents special challenges to the use of SBEM that have not been previously addressed. Earlier tissue preparation methods (Denk & Horstmann, 2004; West, et al., 2010) were modified to enhance ECM staining by incorporating ruthenium red during fixation and primary osmium staining to enhance contrast of structures containing glycosaminoglycans (Luft, 1971a; Luft, 1971b). By incorporating the SEM variable pressure modality, electron charging artifacts were reduced in areas of non-conductive space within the ECM and images could be recorded over a relatively large volume depth. Without the variable pressure, charging resulted in severe image distortion.

Manual and semi-automated segmentation methods were compared using the same raw images from a muscle block. Total time required for segmentation was usually greater for the semi-automated method, although active user time was significantly reduced compared to manual segmentation. Semi-automated segmentation was less able to identify and segment finer details of perimysial collagen cables and fibroblasts when objects with similar intensities were in close proximity and therefore some manual corrections were required (Fig. 2). However, when the object of interest had high contrast to its surroundings, semi-automated segmentation was much faster and more accurate compared to manual segmentation (Fig. 2). The level of detail resulting in this case was greater compared to manual segmentation because Analyze highlights individual voxels belonging to an object while IMOD performs the reconstructions from traced objects. As a result, in Analyze

individual collagen fibrils were differentiated, whereas they were grouped into perimysial collagen cable contours in IMOD and smoothed in the resulting 3D mesh (Fig. 3). Another drawback of meshed manual 3D reconstruction is that meshing errors between images leave gaps in the reconstruction, even if contours are present and accurate on every slice.

This report is the first to visualize 3D skeletal muscle ECM ultrastructure over hundreds of microns. Perimysial collagen cables were identified that have been referred to previously (Borg & Caulfield, 1980; Gillies & Lieber, 2011), but never viewed at this level of detail and certainly not relative to associated structures such as capillaries and fibroblasts. Cables were presumed to be primarily composed of collagen since individual collagen fibrils were morphologically identified within cables based on their size and the classic collagen banding pattern seen when cables were sectioned longitudinally. However, it is possible that other structural proteins, such as elastin (Rowe, 1986), contribute to cable composition and that fibrillar collagen types are heterogeneous among cables. The location and wavy structure of perimysial cables suggest that they may act as the parallel elastic element in skeletal muscle that bears passive load in classic muscle mechanics experiments (Hill, 1953). Unique interactions between perimysial collagen cables and fibroblasts were also observed, suggesting that fibroblasts may be involved in the formation and/or regulation of these perimysial collagen cables.

Characterization of ECM ultrastructure may lead to identification of potential targets for therapy in muscle injury and disease. After inadequate or failed regeneration, skeletal muscle becomes fibrotic resulting in increased muscle stiffness and decreased muscle function. Previous measurements of muscle stiffness correlate relatively poorly with measures of endomysial content such as percent collagen and area fraction of ECM (c.f. Fig. 3 of Lieber & Ward, 2013; Meyer & Lieber, 2012; Smith, et al., 2011). We propose that poor correlations are due to the lack of definition and quantification of ECM structures such as the perimysial cables reported here. Future studies may clarify the functional role of these cables by comparing perimysial cable, number, size and trajectory to passive muscle viscoelastic properties and will be the subject of future publications. Future therapies targeting these structures may reverse the functional deficits resulting from fibrosis.

## Summary

Serial block face scanning electron microscopy for imaging and reconstructing skeletal muscle ECM ultrastructure has been described. Perimysial collagen cables and their physical interaction with fibroblasts and muscle fibers were identified using manual and semi-automated volume segmentation. In future studies, this method will be used to determine how these structures change in response to muscle pathology. By defining the ultrastructure of fibrotic skeletal muscle ECM, therapeutic targets may be identified to reduce fibrosis and associated muscle stiffness in patients with limited function.

## Supplementary Material

Refer to Web version on PubMed Central for supplementary material.

## Acknowledgments

Research reported in this publication was supported by the National Institute of Arthritis and Musculoskeletal and Skin Diseases of the National Institutes of Health under award number R24 HD05083. The National Center for Microscopy and Imaging Research is supported by the National Institute of General Medical Sciences of the National Institutes of Health under award number P41GM103412. The content is solely the responsibility of the authors and does not necessarily represent the official views of the National Institutes of Health. We acknowledge Mason Mackey and Andrea Thor from the National Center for Microscopy and Imaging Research for their assistance with 3View tissue preparation.

## References

Borg TK, Caulfield JB. Morphology of connective tissue in skeletal muscle. Tissue Cell. 1980; 12(1): 197–207. [PubMed: 7361300]

Canty EG, Lu Y, Meadows RS, Shaw MK, Holmes DF, Kadler KE. Coalignment of plasma membrane channels and protrusions (fibripositors) specifies the parallelism of tendon. J Cell Biol. 2004; 165(4):553–563. [PubMed: 15159420]

Denk W, Horstmann H. Serial block-face scanning electron microscopy to reconstruct three-dimensional tissue nanostructure. PLoS Biol. 2004; 2(11):e329. [PubMed: 15514700]

Eisenberg BR, Kuda AM, Peter JB. Stereological analysis of mammalian skeletal muscle. I. Soleus muscle of the adult guinea pig. J Cell Biol. 1974; 60(3):732–754. [PubMed: 4824293]

Gillies AR, Lieber RL. Structure and function of the skeletal muscle extracellular matrix. Muscle Nerve. 2011; 44(3):318–331. [PubMed: 21949456]

Hall CE, Jakus MA, Schmitt FO. An investigation of cross striations and myosin filaments in muscle. Biol Bull. 1946; 90:32–50. [PubMed: 21014276]

Hill AV. The mechanics of active muscle. Proc R Soc Lond B Biol Sci. 1953; 141(902):104–117. [PubMed: 13047276]

Huxley H, Hanson J. Changes in the cross-striations of muscle during contraction and stretch and their structural interpretation. Nature. 1954; 173:973–976. [PubMed: 13165698]

Kremer JR, Mastronarde DN, McIntosh JR. Computer visualization of three-dimensional image data using IMOD. J Struct Biol. 1996; 116(1):71–76. [PubMed: 8742726]

Lieber RL, Ward SR. Cellular mechanisms of tissue fibrosis. 4. Structural and functional consequences of skeletal muscle fibrosis. Am J Physiol Cell Physiol. 2013; 305(3):C241–252. [PubMed: 23761627]

Luft JH. Ruthenium red and violet. I. Chemistry, purification, methods of use for electron microscopy and mechanism of action. Anat Rec. 1971a; 171(3):347–368. [PubMed: 4108333]

Luft JH. Ruthenium red and violet. II. Fine structural localization in animal tissues. Anat Rec. 1971b; 171(3):369–415. [PubMed: 4108334]

Meyer GA, Lieber RL. Skeletal muscle fibrosis develops in response to desmin deletion. Am J Physiol Cell Physiol. 2012; 302(11):C1609–1620. [PubMed: 22442138]

Passerieux E, Rossignol R, Chopard A, Carnino A, Marini JF, Letellier T, Delage JP. Structural organization of the perimysium in bovine skeletal muscle: Junctional plates and associated intracellular subdomains. J Struct Biol. 2006; 154(2):206–216. [PubMed: 16503167]

Purslow PP, Trotter JA. The morphology and mechanical properties of endomysium in series-fibred muscles: variations with muscle length. J Muscle Res Cell Motil. 1994; 15(3):299–308. [PubMed: 7929795]

Rash JE, Ellisman MH. Studies of excitable membranes. I. Macromolecular specializations of the neuromuscular junction and the nonjunctional sarcolemma. J Cell Biol. 1974; 63(2 Pt 1):567–586. [PubMed: 4138515]

Richards AG, Anderson TF, Hance RT. A microtome sectioning technique for electron microscopy illustrated with sections of striated muscle. Exp Biol Med (Maywood). 1942; 51(1):148–152.

Rowe RW. Morphology of perimysial and endomysial connective tissue in skeletal muscle. Tissue Cell. 1981; 13(4):681–690. [PubMed: 7330851]

Rowe RW. Elastin in bovine Semitendinosus and Longissimus dorsi muscles. Meat Sci. 1986; 17(4): 293–312. [PubMed: 22055360]

Sjöstrand F. Electron-microscopic examination of tissues. Nature. 1943; 151:725–726.

Smith LR, Lee KS, Ward SR, Chambers HG, Lieber RL. Hamstring contractures in children with spastic cerebral palsy result from a stiffer extracellular matrix and increased in vivo sarcomere length. J Physiol. 2011; 589(Pt 10):2625–2639. [PubMed: 21486759]

Starborg T, Kalson NS, Lu Y, Mironov A, Cootes TF, Holmes DF, Kadler KE. Using transmission electron microscopy and 3View to determine collagen fibril size and three-dimensional organization. Nat Protoc. 2013; 8(7):1433–1448. [PubMed: 23807286]

Trotter JA, Purslow PP. Functional morphology of the endomysium in series fibered muscles. J Morphol. 1992; 212(2):109–122. [PubMed: 1608046]

West JB, Fu Z, Deerinck TJ, Mackey MR, Obayashi JT, Ellisman MH. Structure-function studies of blood and air capillaries in chicken lung using 3D electron microscopy. Respir Physiol Neurobiol. 2010; 170(2):202–209. [PubMed: 20038456]

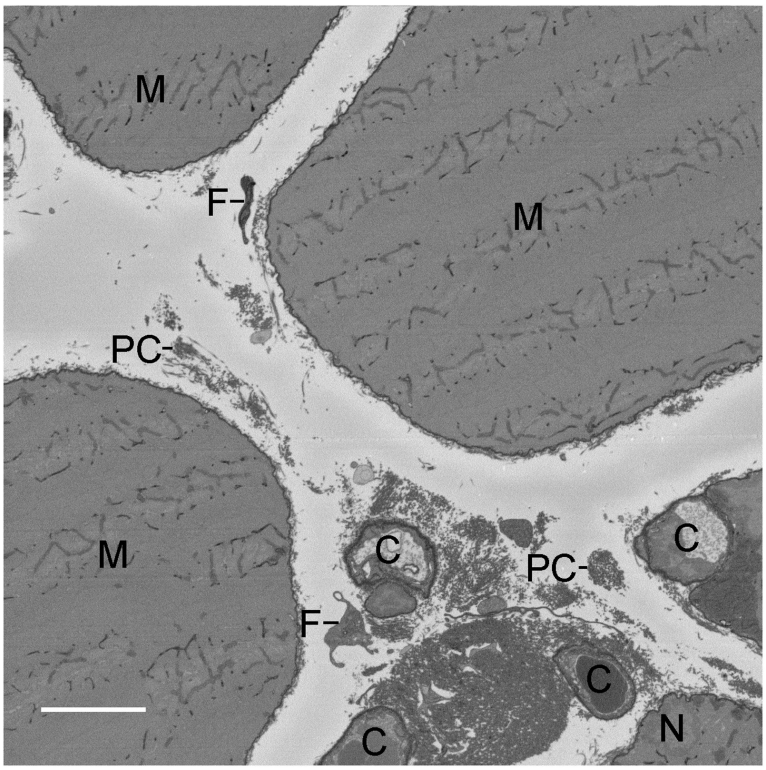


**Figure 1.**

Representative single x-y slice obtained from serial block face scanning electron microscopy (SBEM) of mouse extensor digitorum longus muscle (z=28 μm; z range 0-140 μm). Scale bar = 5 μm. M, myofiber; C, capillary; N, myonucleus; F, fibroblast; PC, perimysial collagen cable.

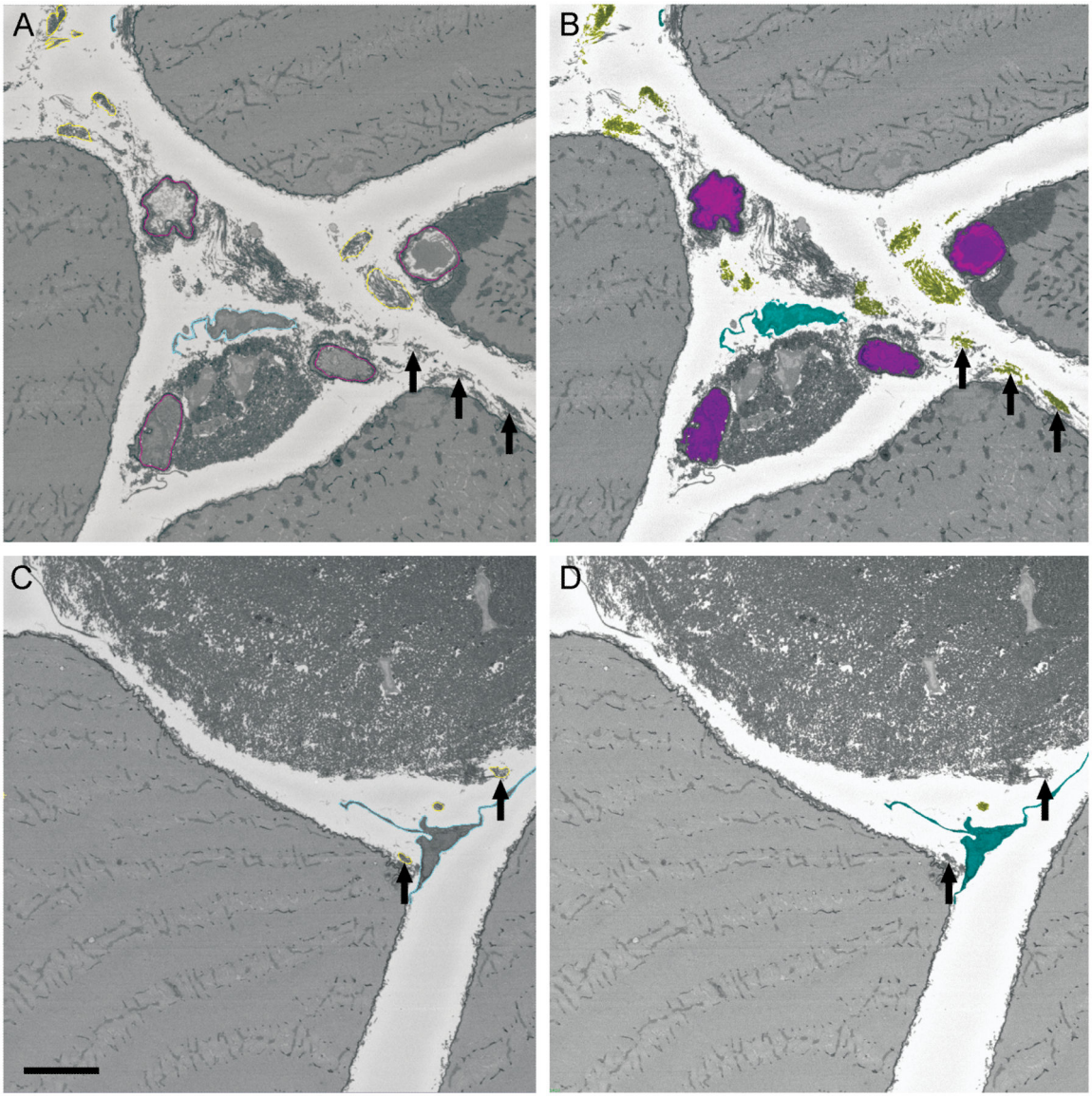


**Figure 2.**

Comparison of two x-y slices from a dataset segmented and reconstructed either manually with IMOD (A and C) or semi-automatically with Analyze (B and D). Manual segmentation created object contours on each slice, whereas semi-automated segmentation highlighted individual voxels within an object. Analyze was able to segment perimysial collagen cables that were highly contrasted compared to their surroundings (B, arrows), while the same cables were too complex to manually define contours with IMOD (A, arrows). Without sufficient contrast, Analyze was unable to distinguish cables from surrounding objects (D, arrows), even when the cables could be followed visually through the volume and segmented manually in IMOD (C, arrows). Capillary, pink; fibroblast, light blue; perimysial collagen cable, yellow. Scale bar = 5 μm.

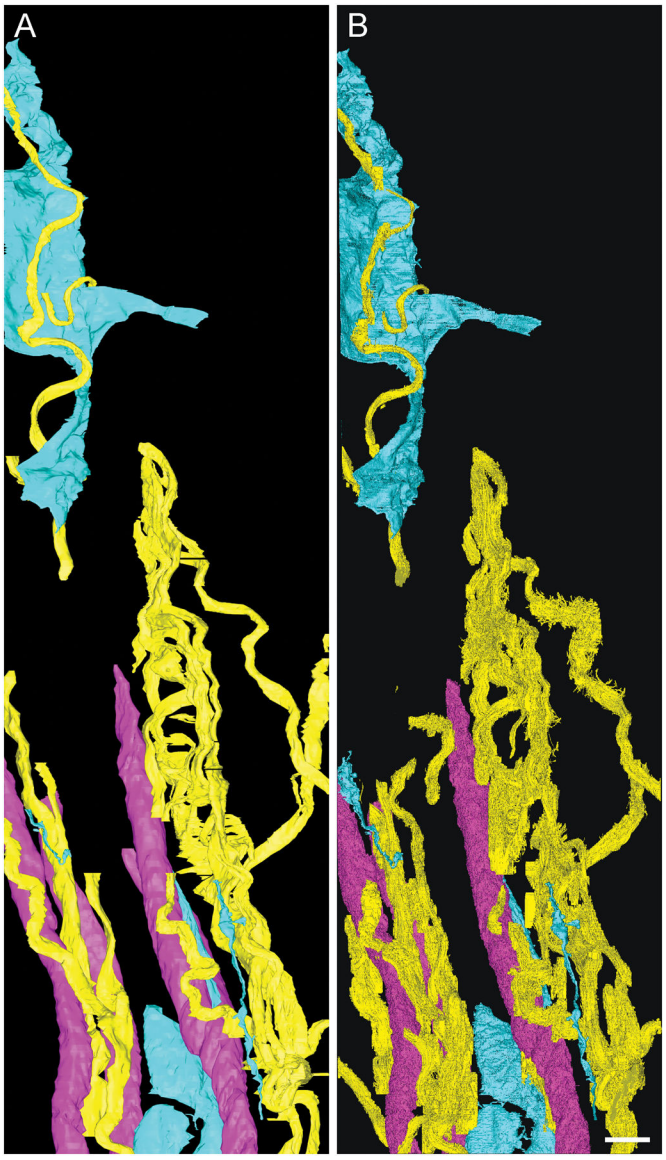


**Figure 3.**

Three-dimensional reconstruction of a dataset segmented manually with IMOD (A) or semi-automatically with Analyze (B) viewed from the x-z plane. Capillary, pink; fibroblast, light blue; perimysial collagen cable, yellow. Scale bar = 5 μm.

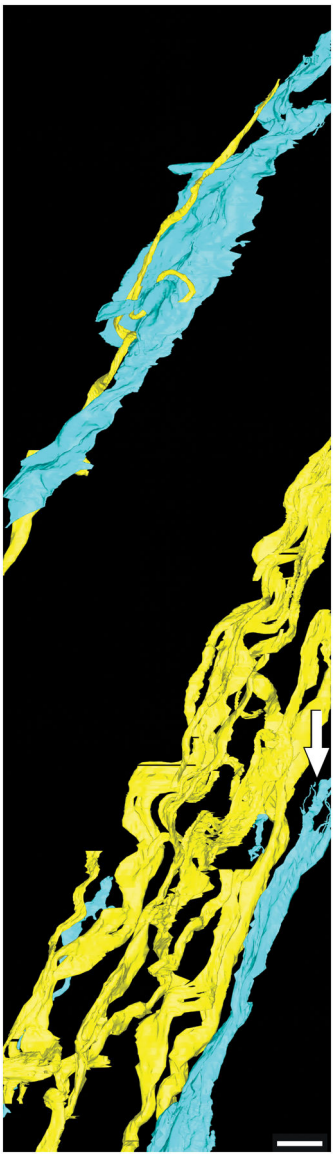

**Figure 4.**

Perimysial collagen cables were found in close proximity to fibroblasts. Thin finger-like projections protruding from the end of a fibroblast were observed (white arrow). The model has been rotated 90° around the z-axis and capillaries were hidden to show fibroblast detail. Fibroblast, light blue; perimysial collagen cable, yellow. Scale bar = 5μm; image obtained by manual reconstruction.